IEEE Access
Multidisciplinary | Rapid Review | Open Access Journal

Received 1 October 2024, accepted 28 October 2024, date of publication 4 November 2024, date of current version 18 November 2024.

Digital Object Identifier 10.1109/ACCESS.2024.3491299

METHODS

Simulation Technique and Mathematical Basis for Faster AC Analysis of Power Factor Correction Boost Converters

KATHERINE A. KIM[1], (Senior Member, IEEE), AND THOMAS G. WILSON JR.[2], (Member, IEEE)
[1]Department of Electrical Engineering, National Taiwan University, Taipei 10617, Taiwan
[2]SIMPLIS Technologies, Portland, OR 97240, USA

Corresponding author: Katherine A. Kim (kakim@ntu.edu.tw)

This work was supported in part by the National Science and Technology Council (NSTC) of Taiwan under Grant 113-2628-E-002-008, and in part by SIMPLIS Technologies.

ABSTRACT Power factor correction (PFC) boost converters are widely used for single-phase industrial ac-dc applications, where simulation is typically used for design and verification. However, running simulations with an ac source at the line frequency (50-60 Hz) can be time-consuming due to the long line period compared to the converter switching period. For PFC converters, the control loop, input impedance, and output impedance are critical to analyze the converter performance. We show that the ac analysis of the control loop and output impedance yields the same frequency response when using an ac and dc voltage source with the same rms value for a single-phase constant-frequency PFC boost converter operating in continuous conduction mode with a high power factor. The mathematical basis for this finding is derived based on a line-averaged rectified converter model. In contrast, for the ac analysis of the input impedance, an ac source must be used for the simulation. A mathematical derivation of this result is presented based on a line-averaged ac-side converter model. From these findings, the use of a dc source for ac analysis of the control loop and output impedance reduced the simulation time to less than 6.8% of that with an ac source.

INDEX TERMS AC analysis, boost converter, input impedance, outer control loop, output impedance, power factor correction, simulation techniques, small-signal modeling.

I. INTRODUCTION

Power factor correction (PFC) circuits in ac-to-dc converters are critical for modern applications because they reduce the harmonics imposed on the grid by nonlinear electronic loads, such as computer power supplies and household appliances [1]. Since harmonic suppression limitations and maximum harmonic currents are regulated by international standards, such as IEC 61000-3-2 [2], commercial ac-to-dc converters with input power over 75 W are generally equipped with PFC circuits. The boost converters are the most common topology used to implement a PFC circuit because they have the advantages of a continuous input current and a straightforward design of the gate driver and control circuits [3].

The associate editor coordinating the review of this manuscript and approving it for publication was Jiaxing Lei.

More recently, higher-power applications in the kW power range are also incorporating PFC circuits, including data centers [4], electric vehicle charging [5] and induction heating systems [6]. The higher the power draw, the larger the potential effect on the power quality of the grid. For example, in applications such as data centers, where there are numerous PFC converters drawing power from the same point of common coupling (PCC) [7], low-frequency stability issues have been identified that are linked to the design of the PFC circuit [8]. The work in [9] showed mathematically that instability can occur after a certain number of PFC converters are connected in parallel to the same PCC. Another study in [10] shows the importance of input impedance analysis for PFC converters to avoid resonance problems when connected to the grid.

To characterize and validate the operation of a PFC converter, ac small-signal analysis (often referred to simply as

ac analysis) is used to understand the converter performance in response to transients and noise [11]. For ac analysis in the frequency domain, we add an ac signal to perturb the system and observe the magnitude and phase of the perturbation signal at the designated output. This is the frequency response that is typically graphed on a Bode plot. Ac analysis demonstrates how the output signal is affected over a wide frequency range and can be used to judge the stability and dynamic response [7], [8], [12]. For a PFC converter, we are primarily concerned with the ac analysis of the control loop, input impedance, and output impedance.

For a converter with feedback control, the frequency characteristics of the closed-loop control transfer function can be used to judge converter stability. For dual-loop feedback control, ac analysis can be performed on the outer control loop [13] to assess the stability and response characteristics of the PFC converter. The frequency characteristics of the input and output impedances are also analyzed, which can affect the devices connected to the input and output of the converter. For example, when two converters are cascaded, the input impedance of the back-end converter should be larger than the output impedance of the front-end converter [14]. If the input impedance of the back-end converter is not high enough, the system may become unstable [15], [16]. Generally, the output impedance of the PFC converter should be smaller than the input impedance of its load [17]. The input impedance of the PFC boost converter is particularly important because it can affect the stability of the PCC from which it draws power, which has become a bigger issue in applications such as data centers with increasing power demands [7], [8].

Simulation is often used to conduct an ac analysis of a PFC converter during the design and verification process. This study utilizes SIMPLIS simulation software (created by SIMPLIS Technologies), a simulation engine used for switched-mode power supply design. SIMPLIS is a powerful design tool to analyze switching systems that can reduce simulation time for transient analysis compared to SPICE, and perform both time-domain and ac analysis with high accuracy. A complete validation of a design that tests various conditions over the input voltage range and output load range could include hundreds of simulation runs. Since the PFC input is the ac grid, each time-domain simulation must capture multiple periods of the line frequency (50 or 60 Hz), which is a much longer time period than that of the boost converter switching period. For example, if a boost converter switches at 100 kHz and the line frequency is 50 Hz, the line period is 2000 times that of the converter switching period. Thus, validating a PFC converter with the ac source at line frequency can take a significant amount of simulation time.

Design engineers and companies can greatly benefit from a faster PFC converter analysis method that does not compromise accuracy. More specifically, if we can use a dc source in place of the ac source without loss of accuracy, it would drastically decrease each simulation run's time. In this article, we use simulation and modeling to analyze when it is effective to use a dc source instead of an ac source in the verification of the PFC boost converter to significantly reduce the simulation time. We also derive the appropriate small-signal models to calculate the transfer functions for the loop gain, input impedance, and output impedance in order to back up the findings mathematically.

The specific PFC boost converter used in this study is shown in Fig. 1, where the rated power is 200 W, output voltage is 400 V, and input voltage ranges from 105 to 265 V rms. The PFC boost converter employs average current mode (ACM) control, which can achieve a high power factor, supply current with low harmonics over a wide range of input voltages and load currents, and yield high efficiency [18], [19]. This design is an example from an industrial application, but component values are not necessarily fully optimized. This shows that the simulation technique presented here can be used to analyze the converter throughout the design and optimization process. This study focuses on single-phase PFC boost converters that are assumed to operate in continuous conduction mode (CCM) over a full half-line cycle, and the control is implemented such that a high power factor is achieved over the operating range.

Ac analysis in SIMPLIS is used to investigate the single-phase PFC boost converter operating in CCM with high power factor and show that the outer control loop (hereafter, simply called *control loop*) and output impedance measured with an ac source are equivalent to when a dc source set to the rms value of the ac source is used. In contrast, the input impedance results with an ac and dc source are shown to differ, which has not yet been investigated in the existing literature. The contributions of this work are: 1) verifying that the frequency responses for the control loop and output impedance are the same (excluding the region around twice the line frequency) for an ac source and a dc source with the same rms value; 2) quantifying that this dc-input-source method can reduce simulation time to less than 7% compared to using an ac input source; 3) deriving the small-signal model referred to as the line-averaged rectified model for the control loop and output impedance to prove why the RMS value can be used as the equivalent dc source value; and 4) deriving the small-signal model referred to as the line-averaged ac-side model for the input impedance to explain why the same dc-input-source method cannot be used for the input impedance.

The rest of the article is organized as follows. Section II describes the setup and design of the single-phase boost converter investigated in this work. Section III provides the simulated frequency response plots and simulation times of the control loop, output impedance, and input impedance when an ac and dc source with the same rms values are used. Section IV gives a mathematical derivation of the line-averaged rectified converter model, for the control loop and output impedance, and a separate line-averaged ac-side converter model, for the input impedance. This derivation shows why a dc source equivalent to the rms value of the ac source can be used for the line-averaged rectified converter

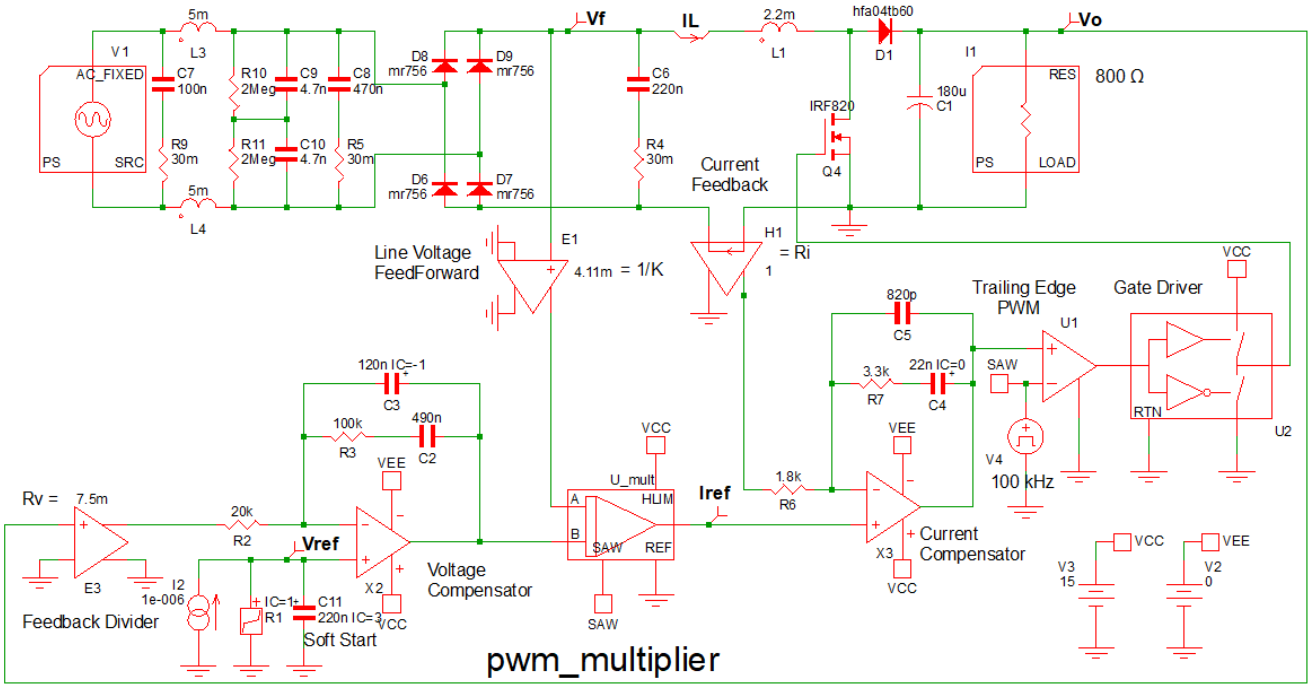

FIGURE 1. Schematic diagram in SIMPLIS of a single-phase boost PFC converter with ACM control. The output voltage is fed back through a voltage compensator and then goes to pin B of the multiplier. The rectified source voltage is fed through a multiplier to pin A of the multiplier. The output of the multiplier forms the moving reference for the current compensator that takes the feedback of the inductor current and produces the PWM signal for the converter.

model but not the line-averaged ac-side converter model. Section V discusses the significance and limitation of the findings and Section VI concludes the article. A full list of simulation parameters and links to the simulation files used in this work are provided in the appendix.

II. PFC BOOST CONVERTER DESIGN

This study applies ac analysis to a single-phase PFC boost converter using ACM control [13] in SIMPLIS, as shown in Fig. 1. ACM control is a dual-loop control that consists of an output voltage and an inductor current feedback loop to ensure that the input current waveform tracks the ac input voltage waveform. In Fig. 1, output voltage is multiplied by the proportion of the voltage divider, R_v and is compared to the reference voltage, V_{ref}, in the voltage compensator. The output of the voltage compensator is then multiplied by the boost input voltage divided by the constant K. The resulting product of i_{ref} acts as the reference value for the current control, which follows the shape of the rectified ac input voltage waveform. The inductor current is multiplied by a voltage divider proportion, R_i, and then it is compared to i_{ref} through the current compensator, as shown in Fig. 1. Then, the current compensator output is compared to a sawtooth waveform operating at the switching frequency of 100 kHz, which creates the PWM signal that drives the MOSFET of the boost converter via a gate driver.

The converter is designed to operate with an input voltage range of 105 V to 265 V rms at 50 Hz line frequency. The input filter reduces the noise created by the converter from going back into the ac line. The full-bridge rectifier converts the ac waveform into a full-wave rectified waveform, and then the boost converter steps up the output voltage to 400 V at a rated power of 200 W. The specifications of the boost converter and its components are summarized in Table 1. The single-phase boost converter is assumed to operate in CCM over the full half-line cycle (possibly excluding a few switching cycles during the zero-crossing of the ac line) and the power factor is greater than 98% in the input voltage range at full load.

TABLE 1. Converter design specifications.

Specification	Value
AC input voltage	105 - 265 V rms
AC line frequency	50 Hz
DC output voltage	400 V
DC output current	0.5 A
Output power	200 W
Switching frequency	100 kHz

III. FREQUENCY RESPONSE WITH DC AND AC SOURCES

Ac analysis is a method used to assess the frequency response of a system. The frequency response can be calculated by superimposing a perturbation on a defined input signal and measuring the amplitude and phase of the perturbation at the defined output signal. In an experiment, frequency response measurements can be limited in accuracy due to poor

signal-to-noise conditions. SIMPLIS simulation can be an effective tool for determining the frequency response even down to very low frequencies, which would be challenging to measure experimentally. Using simulation, we examine the frequency responses of the control loop, output impedance, and input impedance over a wide frequency range for a single-phase PFC boost converter.

The early work in [20] and [21], showed that the frequency response of a PFC converter can be directly measured in the experiment using an ac source. In [20], the experimental control loop results were compared using an ac source and a dc source, and it was found that their frequency responses were approximately the same when the dc source was set to the rms value of the ac source. We also applied the dc source technique to the relevant frequency responses of the single-phase PFC boost converter and found that using a dc source at the rms value of the ac source yields the same response for the control loop and output impedance, but not the input impedance. The simulated results for both the ac and dc sources are as follows.

A. CONTROL LOOP

For the control loop Bode plot, comparison results for an ac and dc source are shown in Fig. 2, where three different input rms voltages were tested: 105 V, 185 V, and 265 V. The solid curves (with circles) are the simulation results with an ac input source and the dashed curves are the simulation results with a dc input source at the rms value. Both source types show well-matched results over the full frequency range. The control loop Bode plot results are the same with an ac source and with a dc source at the equivalent rms value. System stability and dynamic performance can be analyzed using the control loop transfer function. The corresponding crossover frequencies for the outer loop were 3, 9, and 15 Hz, respectively; while the phase margins were 67, 56, and 44 degrees.

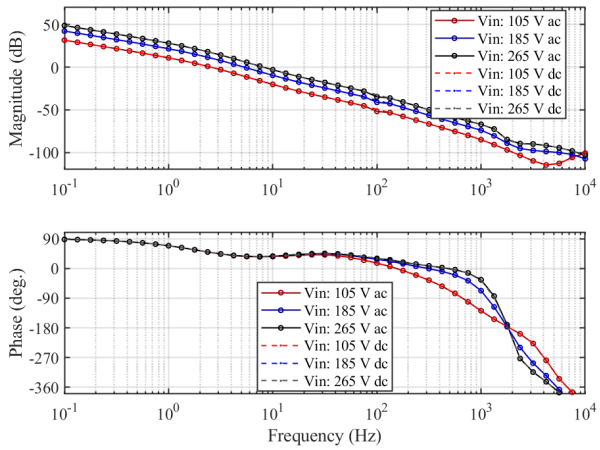

FIGURE 2. Bode plot of the outer control loop simulated with an ac source at rms voltages of 105, 185, and 265 V and a dc source set to the same value as the three rms values. The output voltage is 400 V at 0.5 A with a resistive load of 800 ohms for all input voltage cases.

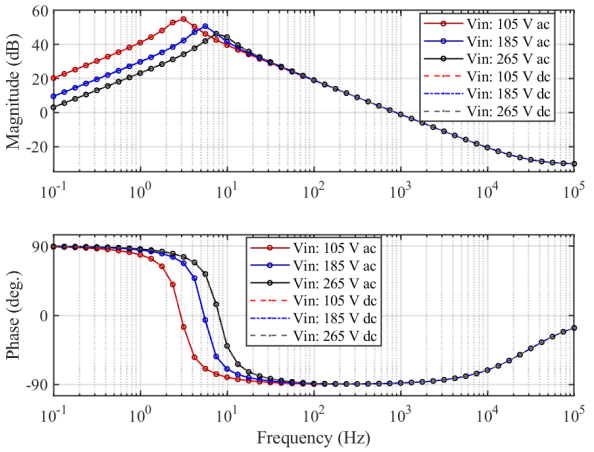

FIGURE 3. Frequency response of the output impedance simulated with an ac source at rms voltages of 105, 185, and 265 V and a dc source set to the same value as the three rms values. The output voltage is 400 V at 0.5 A with a resistive load of 800 ohms for all input voltage cases.

B. OUTPUT IMPEDANCE

The output impedance frequency response results are compared when using an ac and dc source, as shown in Fig. 3, for the three different input rms voltages of 105 V, 185 V, and 265 V. The solid curves (with circles) are the PFC output impedance simulation results with an ac input source and the dashed curves are the results with a dc input source. In Fig. 3, both curves are well matched over the full frequency range (0.1 Hz to 100 kHz).

C. INPUT IMPEDANCE

In a PFC converter, the low-frequency input impedance should act resistively such that any noise or distortion in the voltage waveform would produce a proportional in-phase response in the current waveform [22]. For the simulated input impedance frequency response, the results using an ac and dc source are compared, as shown in Fig. 4, for the input rms voltages of 105 V, 185 V, and 265 V. The solid curves (with circles) show the PFC input impedance simulation results with an ac input source. At low frequency, the magnitude is constant and the phase is 0°, such that the input exhibits the desired purely resistive characteristics. There is a magnitude peak around 50 Hz (line frequency) where the ac perturbation signal interferes positively with the line frequency. The dashed curves in Fig. 4 are the PFC input impedance simulation results with a dc input source. With the dc source input, the low-frequency phase is −180°, which means that the input acts as an effective negative impedance, similar to a boost converter that provides power to a constant-power load. Notice that above 1 kHz the characteristics of the input filter dominate both the dc and ac curves.

The frequency response results show that using a dc source at the rms value of the ac source gives the same results for the outer loop and output impedance, but not at low frequencies for the input impedance. Hence, for the frequency response of the control loop and output impedance, a dc source at the ac

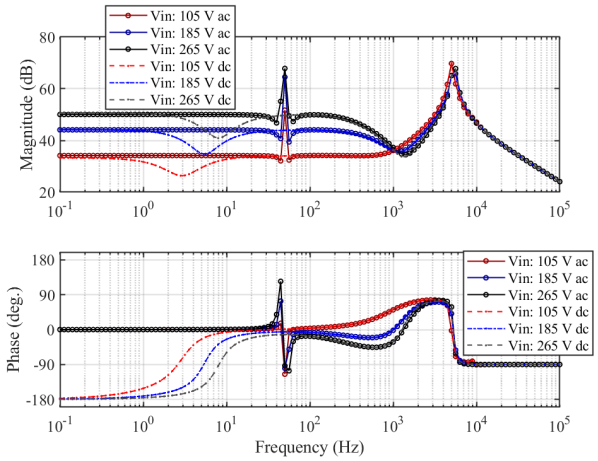

FIGURE 4. Frequency response of the input impedance simulated with an ac source at rms voltages of 105, 185, and 265 V and a dc source set to the same value as the three rms values. The output voltage is 400 V at 0.5 A with a resistive load of 800 ohms for all input voltage cases.

source's rms value for a single-phase PFC boost converter (in CCM and with a high power factor) yields the same results as with an ac source. Note that these findings are valid for full-load conditions, but the ac-source and dc-source results can begin to diverge for some control schemes under light-load conditions, which requires further study.

D. SIMULATION TIMES

For the simulations of the control loop, output impedance, and input impedance frequency responses, Table 2 shows each simulation time using an ac source (at 256 V rms) and a dc source (at 256 V); the ac analysis simulation was run from 0.1 to 100 kHz with 15 points per decade (using SIMPLIS version 8.4). Frequency response simulations with an ac source took more than 4 minutes and 38 seconds to measure, while those with the dc source took 19 seconds (6.8% of the ac-source case). In validating the single-phase PFC boost converter design operating in CCM with a high power factor, we can use a dc input voltage source to significantly reduce simulation time. However, the same cannot be said for the input impedance, as the frequency characteristics do not match, as shown in Fig. 4. Thus, the small-signal model for the input impedance requires further investigation to accurately model and interpret the simulation results obtained with an ac and dc source. An ac source should be used to properly validate the input impedance of a PFC boost converter. In other words, attempting to reduce the simulation time by using a dc source does not yield an accurate input impedance result.

TABLE 2. Simulation time with AC and DC sources (Input voltage: 256 V, Frequency range: 0.1 to 100 kHz, points per decade: 15).

Simulation	AC Source (265 V rms)	DC Source (265 V)
Control Loop	4 min. 38 s	19 s
Output Impedance	4 min. 43 s	19 s
Input Impedance	5 min. 3 s	19 s

IV. SMALL-SIGNAL MODELING

In this section, the small-signal models for the control loop, output impedance, and input impedance transfer functions are derived. The results are then compared to the simulation results found using SIMPLIS. Line averaging will be applied to a rectified model of the PFC boost converter for the control loop and output impedance ac analysis, and it will be applied to an ac-side model for the input impedance ac analysis.

A. LINE-AVERAGED RECTFIED MODEL

A PFC boost converter with an input filter is a complex system to model, but we can make a number of assumptions to simplify the system while maintaining the accuracy of the small-signal model. This model will be used for both the control loop and output impedance modeling, but not for the input impedance. The schematic of the rectified PFC boost converter used for this model is shown in Fig. 5 and is derived based on the following key assumptions.

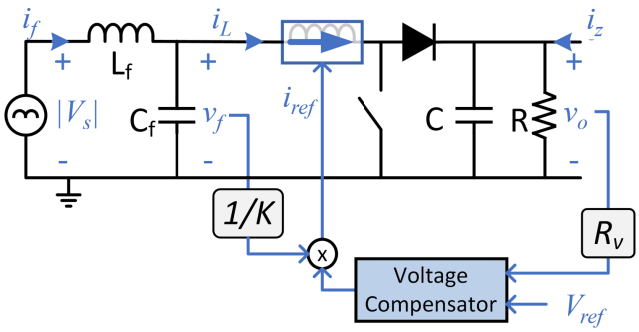

FIGURE 5. System diagram showing the rectified PFC boost converter with a simplified two-component input filter. This model is averaged over half the line period to derive the small-signal models of the control loop and output impedance.

1) ASSUMPTION 1

The first key assumption is that the input to the boost PFC converter is a rectified sinusoidal waveform. In a sense, this model is viewing the system from the boost converter's side such that the input to the converter is already rectified. Although the rectifier is actually after the line filter, the filter components are designed to attenuate frequencies above twice the line frequency; hence, they can be moved after the rectified signal without compromising the integrity of the model. The ac source voltage is defined as

$$V_s = \sqrt{2} V_{rms} \sin(2\pi f_l t) \tag{1}$$

where V_{rms} is the rms value of the source voltage, f_l is the line frequency, and t is time. Then the rectified source voltage is the absolute value of the sinusoidal voltage, which

is expressed as

$$|V_s| = |\sqrt{2}V_{rms}\sin(2\pi f_l t)| \tag{2}$$

2) ASSUMPTION 2

The second key assumption is that the input filter is simplified to a series inductance L_f and a parallel capacitance C_f before the boost converter. For this analysis, the series resistances of the filter elements are ignored. For this specific design, the series filter inductance is modeled as

$$L_f = L_3 + L_4 \tag{3}$$

and the parallel filter capacitance is modeled as

$$C_f = C_6 + C_8 \tag{4}$$

where all parameters are listed in Table 3 of the appendix.

3) ASSUMPTION 3

The third key assumption is that the inductor current perfectly matches the current reference i_{ref}. This assumption can generally be made for PFC converters because the current compensation is designed to react much faster than the voltage compensation so that the inductor current can follow the rectified sinusoidal reference. Mathematically, this means that the inductor current i_L is defined by

$$i_L = \frac{v_f}{K}v_{con} = i_{ref} \tag{5}$$

where v_f is the rectified voltage after it has gone through the input filter, K is a control parameter, and v_{con} is the output signal of the voltage compensation. By assuming perfect current control, we also reduce the order of our model since the inductor no longer has a derivative component, which also simplifies our overall model.

4) ASSUMPTION 4

The fourth key assumption is that the boost converter operates in CCM and has no losses. Thus, the follow voltage gain equation is assumed to be true

$$(1-d) = \frac{v_f}{v_o} \tag{6}$$

where d is the on-time duty ratio of the boost converter, v_f is the voltage at the input of the boost converter stage, and v_o is the output voltage of the boost converter.

5) DYNAMIC EQUATIONS

First, we start with the differential equations of the inductor and capacitors in the rectified boost converter model. The dynamic states for this model are the input filter inductor i_f, input filter capacitor voltage v_f, and output capacitor voltage v_o. The dynamic equation for the input filter inductor L_f is

$$L_f\frac{di_f}{dt} = |V_s| - v_f \tag{7}$$

where $|V_s|$ is the rectified source voltage defined in (2). The dynamic equation for the input filter capacitor C_f is

$$C_f\frac{dv_f}{dt} = i_f - i_L \tag{8}$$

where i_L is the boost converter's inductor current. Note that due to Assumption 3, i_L is a state but not a dynamic state in this model and therefore does not have a differential equation. The dynamic equation for the output capacitor C is

$$C\frac{dv_o}{dt} = i_L(1-d) - \frac{v_o}{R} + i_z \tag{9}$$

where R is the load resistance and i_z is the injected current used to measure the output impedance.

Because we assume that the inductor current perfectly matches the reference value (Assumption 3), we can substitute (5) into (8), which yields

$$C_f\frac{dv_f}{dt} = i_f - \frac{v_f}{K}v_{con} \tag{10}$$

Using Assumption 3 again and assuming the converter operates in CCM (Assumption 4), we can substitute (5) and (6) into (9), which yields

$$C\frac{dv_o}{dt} = \frac{1}{K}\frac{v_f^2}{v_o}v_{con} - \frac{v_o}{R} + i_z \tag{11}$$

6) LARGE-SIGNAL VALUES

Next, we examine the large-signal values of the variables in the model. In addition to the state variables (i_f, v_f, v_o), the control signal v_{con} and the injected load current i_z are also variables in the model. The large-signal values for each of the variables are denoted with capital letters. To determine the large-signal relationships when the dynamic states are at equilibrium, the derivatives of the dynamic states are set to 0, such that (7) and (11), respectively, become

$$0 = |V_s| - V_f \tag{12}$$

$$0 = \frac{1}{K}\frac{V_f^2}{V_o}V_{con} - \frac{V_o}{R} + I_z \tag{13}$$

Next, since i_z is an injected ac signal over the load terminals to measure the output impedance, its large-signal current value is equivalent to an open circuit such that $I_z = 0$. Then, from (13), we find that

$$V_{con} = \frac{KV_o^2}{RV_f^2} \tag{14}$$

holds true for large signals, which will be used later.

7) LINEARIZATION

Next, we linearize (7), (10), and (11) around the large-signal equilibirum values to get the equations in terms of the

small-signal variables (denoted with hats), which yields

$$L_f \frac{d\hat{i}_f}{dt} = -\hat{v}_f \tag{15}$$

$$C_f \frac{d\hat{v}_f}{dt} = \hat{i}_f - \frac{V_{con}}{K}\hat{v}_f - \frac{V_f}{K}\hat{v}_{con} \tag{16}$$

$$C\frac{d\hat{v}_o}{dt} = \frac{2V_{con}V_f}{KV_o}\hat{v}_f - \left(\frac{V_{con}V_f^2}{KV_o^2} + \frac{1}{R}\right)\hat{v}_o + \frac{V_f^2}{KV_o}\hat{v}_{con} + \hat{i}_z \tag{17}$$

We can substitute V_{con} from (14), into (16) and (17), and simplify to get

$$C_f \frac{d\hat{v}_f}{dt} = \hat{i}_f - \frac{V_o^2}{RV_f^2}\hat{v}_f - \frac{V_f}{K}\hat{v}_{con} \tag{18}$$

$$C\frac{d\hat{v}_o}{dt} = \frac{2V_o}{RV_f}\hat{v}_f - \frac{2}{R}\hat{v}_o + \frac{V_f^2}{KV_o}\hat{v}_{con} + \hat{i}_z \tag{19}$$

8) AVERAGEING OVER HALF THE LINE PERIOD

Now, we take the average over half the line period for (15), (18), and (19). This only affects the large-signal terms that are not constant dc values, which is V_f. Notice that (15) is not affected by taking the average over half the line period and remains the same.

Substituting (2) and (12) into the term V_f^2 yields

$$V_f^2 = \left[\sqrt{2}V_{rms}\sin(2\pi f_l t)\right]^2 \tag{20}$$

averaging (20) over half the line period is expressed as

$$\bar{V_f^2} = 2f_l \int_0^{\frac{1}{2f_l}} \left[\sqrt{2}V_{rms}\sin(2\pi f_l t)\right]^2 \tag{21}$$

Recall that V_{rms} is the rms value of the input voltage defined in (1). Based on the definition of rms, the right side of (21) can be put in terms of V_{rms} which yields

$$\bar{V_f^2} = V_{rms}^2 \tag{22}$$

Conversely, V_f averaged over half the line period is not equivalent to the RMS value, so it is denoted as $\bar{V}_f$. Substituting these values into (18) and (19) yields the half-line-averaged small-signal equations which are

$$C_f \frac{d\hat{v}_f}{dt} = \hat{i}_f - \frac{V_o^2}{RV_{rms}{}^2}\hat{v}_f - \frac{\bar{V}_f}{K}\hat{v}_{con} \tag{23}$$

$$C\frac{d\hat{v}_o}{dt} = \frac{2V_o}{R\bar{V}_f}\hat{v}_f - \frac{2}{R}\hat{v}_o + \frac{V_{rms}{}^2}{KV_o}\hat{v}_{con} + \hat{i}_z \tag{24}$$

9) LAPLACE TRANSFORM

Finally, the Laplace transform is applied to (15), (23), and (24), and like terms are gathered, which, respectively, yields

$$L_f s\hat{i}_f = -\hat{v}_f \tag{25}$$

$$\left(C_f s + \frac{V_o^2}{RV_{rms}{}^2}\right)\hat{v}_f = \hat{i}_f - \frac{\bar{V}_f}{K}\hat{v}_{con} \tag{26}$$

$$\left(Cs + \frac{2}{R}\right)\hat{v}_o = \frac{2V_o}{R\bar{V}_f}\hat{v}_f + \frac{V_{rms}{}^2}{KV_o}\hat{v}_{con} + \hat{i}_z \tag{27}$$

These equations represent the line-averaged (over half the line period) small-signal model for the rectified boost converter and will be used to derive the outer loop and output impedance transfer functions.

B. CONTROL LOOP TRANSFER FUNCTION

To understand the control loop, we can follow the output voltage feedback signal in Fig. 1. First, the voltage signal is scaled down by R_v and then compared to a set reference voltage when fed into the voltage compensator. The output of the voltage compensator is v_{con}, which is one of the variables in the derived rectified PFC boost converter model. The small-signal diagram of this control loop is shown in Fig. 6. Note that the negative before the voltage compensator is because the measured signal is subracted from a fixed reference. Then, the transfer function of the control loop T, can be expressed as

$$T = -G_{vcon}R_vG_{vc} \tag{28}$$

where G_{vcon} is the transfer function of the control signal to the output voltage for the rectified PFC boost converter model, R_v is a scalar value given in Table 3, and G_{vc} is the transfer function of the voltage compensation.

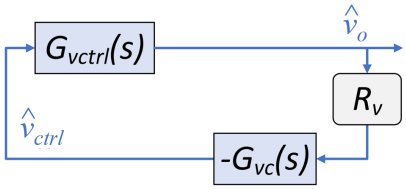

FIGURE 6. Small-signal diagram used to analyze the control loop of the PFC boost converter. To determine the transfer function, the loop of the diagram can be broken at $\hat{v}_{con}$, such that the perturbation signal is inserted before G_{vcon} and the response is measured after the voltage compensator.

1) CONVERTER CONTROL-TO-OUTPUT TRANSFER FUNCTION

To derive the control-signal-to-output-voltage transfer function, we set $\hat{v}_{con}$ as our input, $\hat{v}_o$ as our output, and other non-state variables to zero, which is $\hat{i}_z = 0$. Then, the system of three equations given in (25), (26), and (27) can be used to solve for the transfer function in terms of $\hat{v}_{con}$ and $\hat{v}_o$. After careful calculation, the control-signal-to-output-voltage transfer function for the rectified PFC boost converter

can be expressed as

$$G_{vcon} = \frac{RV_{rms}{}^2}{2KV_o} \frac{L_f C_f s^2 - \frac{V_o^2}{RV_{rms}{}^2} L_f s + 1}{\left(\frac{s}{\omega_p} + 1\right)\left(L_f C_f s^2 + \frac{V_o^2}{RV_{rms}{}^2} L_f s + 1\right)} \tag{29}$$

where the pole originating from the boost converter power stage ω_p is

$$\omega_p = \frac{2}{RC} \tag{30}$$

Notice that in G_{vcon}, the only value related to the voltage source is V_{rms}. This means that the small-signal model is the same as if the voltage source were a dc source set to the rms value of the original ac source.

2) VOLTAGE COMPENSATOR TRANSFER FUNCTION

The transfer function for the voltage compensator G_{vc} can be derived as in [13] and expressed as

$$G_{vc} = \frac{K_{vc}}{s} \frac{\left(1 + \frac{s}{\omega_{zvc}}\right)}{\left(1 + \frac{s}{\omega_{pvc}}\right)} \tag{31}$$

where the gain term is

$$K_{vc} = \frac{1}{R_2(C_2 + C_3)} \tag{32}$$

the zero ω_{zvc} is

$$\omega_{zvc} = \frac{1}{R_3 C_2} \tag{33}$$

and the pole ω_{pvc} is

$$\omega_{pvc} = \frac{1}{R_3 \frac{C_2 C_3}{C_2 + C_3}} \tag{34}$$

This voltage compensator transfer function in (31) along with the boost converter transfer function in (29) can be substituted into (28) to find the control loop transfer function T.

C. CONTROL LOOP MODEL COMPARISON

The small-signal model for the control loop, given in (28), can be used to generate the frequency response. Fig. 7 shows the Bode plot of the outer loop frequency response, comparing the derived model and with the measured simulation results using an ac source with rms voltages of 105 V, 185 V, and 265 V. The rectified line-averaged model and simulation results are well matched up to 50 Hz, above the cross-over frequency for all source voltages. Around the rectified line frequency of 100 Hz, the simulation slightly diverges from the model because the line-averaged model does not consider interactions with the line frequency. Above 500 Hz, the effects of input filter are observed, indicated by the drop in frequency; since the input filter in the model is simplified, there is some divergence, but that gain at these frequencies is quite low, such that the model is still effective for evaluating the control loop.

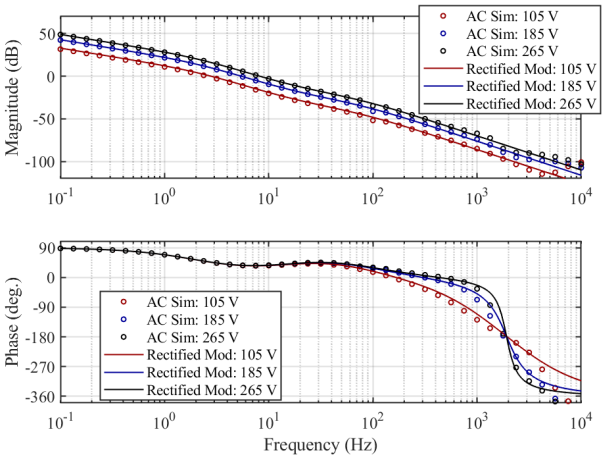

FIGURE 7. Frequency response of the outer control from the simulation (ac source) for rms voltages of 105, 185, and 265 V compared to the small-signal models with the dc value set to the same value as the three rms values. The output voltage is 400 V at 0.5 A with a resistive load of 800 ohms for all input voltage cases.

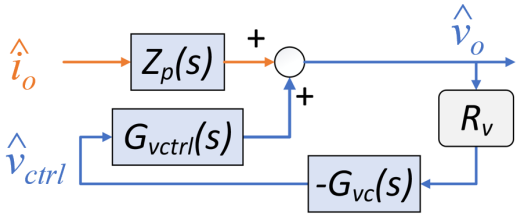

FIGURE 8. Small-signal diagram used to analyze the output impedance of the PFC boost converter, where the perturbation signal is the small-signal output current $\hat{i}_o$ and the response is measured at the output voltage $\hat{v}_o$.

D. OUTPUT IMPEDANCE TRANSFER FUNCTION

To understand the output impedance, we can again refer to Fig. 1 and look at the output side. A small-signal current $\hat{i}_z$ injected in parallel with the resistor load and observe the small-signal changes in the output voltage $\hat{v}_o$. The boost converter has some output impedance properties based on the converter components, and since the converter employs feedback control, the effect of feedback also needs to be taken into account for small-signal modeling. The small-signal diagram of the output impedance is shown in Fig. 8, where both output impedance of the open-loop converter (plant), Z_p, and the feedback loop are illustrated. Based on this model, the transfer function of the boost converter's output impedance is expressed as

$$Z_o = \frac{Z_p}{1 - T} \tag{35}$$

where Z_p is the converter's open-loop output impedance transfer function and T is the control loop transfer function given in (28).

1) CONVERTER OUTPUT IMPEDANCE TRANSFER FUNCTION

To derive the open-loop converter output impedance transfer function, we set $\hat{i}_z$ as our input, $\hat{v}_o$ as our output, and other nonstate variables to zero, which is $\hat{v}_{con} = 0$. Then, we examine the system of three equations given in (25), (26), and (27). We see that (27) contains both the input and output variables, but (25) and (26) only contain the state variables $\hat{i}_f$ and $\hat{v}_f$; this means that the only valid solution the yields the transfer function is for $\hat{i}_f = 0$ and $\hat{v}_f = 0$. This also makes sense intuitively because the input filter components are effectively decoupled from the output side when the inductor current of the boost converter is assumed to be perfect (Assumption 3), so they do not affect the output impedance in this model. Thus, (27) can be used to solve for the transfer function in terms of $\hat{i}_z$ and $\hat{v}_o$, such that open-loop PFC boost's output impedance transfer function can be expressed as

$$Z_p = \frac{R}{2}\frac{1}{\frac{s}{\omega_p}+1} \tag{36}$$

where ω_p is the pole from the boost converter power stage given in (30). The converter transfer function in (36) can be substituted into (35) to determine the output impedance of the closed-loop converter.

E. OUTPUT IMPEDANCE MODEL COMPARISON

The small-signal model for the output impedance, given in (35), can be used to generate the frequency response. Fig. 9 shows the output impedance frequency response, comparing the derived model with the simulation results using an ac source at rms voltages of 105 V, 185 V, and 265 V. As shown in Fig. 9, the line-averaged rectified model and simulation results are well matched for the gain up to 10 kHz and for the phase up to 1 kHz. The simulation slightly diverges from the model above these frequencies because the non-idealities of the current control loop, which are ideal in the model (Assumption 3) start to be observed. However, the gain where the divergence occurs is at very low gain, so the model is still effective for evaluating the output impedance.

F. LINE-AVERAGED AC-SIDE MODEL

For examining signals before the full-wave rectifier, such as the input impedance, we cannot assume the rectified model given in Section IV-A. For this ac-side model, we can also make a number of assumptions to simplify the system while maintaining the accuracy of the small-signal model. This model is used only for the input impedance. The schematic of the ac-side input filter and the PFC boost converter used for this model is shown in Fig. 10 and is derived based on the following key assumptions.

1) ASSUMPTION 5

The first key assumption for this model is that the input to the boost PFC converter is a sinusoidal waveform. In a sense, this model views the system from the ac sources side such

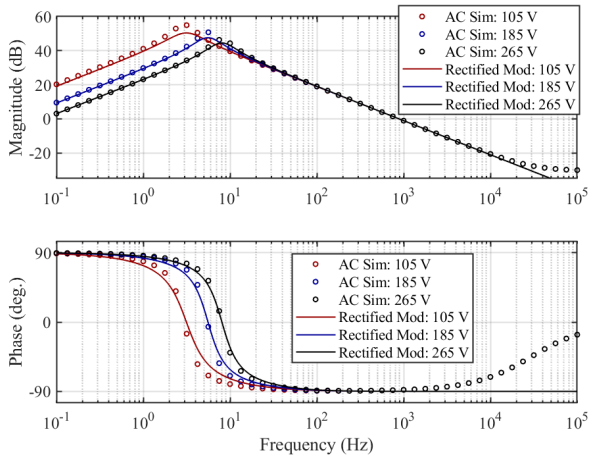

FIGURE 9. Frequency response of the output impedance from the simulation (ac source) for rms voltages of 105, 185, and 265 V compared to the small-signal model with the dc value set to the same values as the three rms values. The output voltage is 400 V at 0.5 A with a resistive load of 800 Ohms for all input voltage cases.

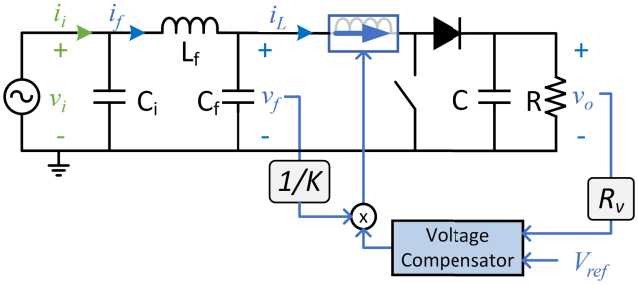

FIGURE 10. System diagram showing the PFC boost converter viewed from the ac-side with a simplified three-component input filter. This model is averaged over half the line period to derive the small-signal model for the input impedance.

that only the boost converter stage is rectified. The ac source voltage is defined in (1).

2) ASSUMPTION 6

The second key assumption for this model is that the input filter is simplified to three components: an input capacitor C_i, a series inductance L_f, and parallel capacitance C_f before the boost converter. Again, the series resistances of the filter elements are ignored. For this specific design, the input filter capacitance is modeled as

$$C_i = C_7 \tag{37}$$

where all parameters are listed in Table 3 of the appendix. The series filter inductance is given in (3) and the parallel filter capacitance is given in (4).

3) ASSUMPTION 3

The third key assumption for this model is the same as Assumption 3 (inductor current perfectly matches the current reference) given in Section IV-A3.

4) ASSUMPTION 4

The fourth key assumption for this model is the same as Assumption 4 (boost converter operates in CCM) given in Section IV-A4.

5) DYNAMIC EQUATIONS

First, we start with the differential equations of the input filter and boost converter model from the ac source side. The dynamic states for this model are the input filter capacitor voltage v_i, filter inductor i_f, and parallel filter capacitor voltage v_f. The dynamic equation for the input filter capacitor C_i is

$$C_i \frac{dv_i}{dt} = i_i - i_f \tag{38}$$

where i_i is the input current from the ac source. The dynamic equation for the filter inductor L_f is

$$L_f \frac{di_f}{dt} = v_i - v_f \tag{39}$$

The dynamic equation for the parallel filter capacitor C_f is the same as in (8), but note that in this model, the boost converter's inductor current i_L is seen from the unrectified side. Due to Assumption 3, i_L is a non-dynamic state governed by (5), where v_f is also seen from the unrectified side. Although (5) is not a dynamic equation, it can still be used to determine the impedance in the following steps.

6) LARGE-SIGNAL VALUES

Next, we examine the large-signal values of the variables in the model. In addition to the state variables (v_i, i_f, v_f, i_L), the input source current i_i is also a variable in the model. The large-signal values are denoted with capital letters. To determine the large-signal relationships at equilibrium, the derivatives of the dynamic states are set to 0, such that (39) becomes

$$0 = V_s - V_f \tag{40}$$

From (40) we see that

$$V_f = V_s \tag{41}$$

holds true for large signals. Note that the equilibrium relationships for (38) and (8) are not used in the following analysis, so their equations are omitted. Although the output capacitor of the boost converter is not considered a dynamic state in this analysis because it is decoupled from the input side, its large-signal equilibrium values given in (13) are still valid for this model (assuming $I_z = 0$). Then, it follows that (14) also holds for this model. Substituting (41) into (14) yields

$$V_{con} = \frac{KV_o^2}{RV_s^2} \tag{42}$$

which will be used in the next step.

7) LINEARIZATION

Next, we linearize (38), (39), (8), and (5) around the large-signal equilibirum values to get the equations in terms of the small-signal variables, which yields

$$C_i \frac{d\hat{v}_i}{dt} = \hat{i}_i - \hat{i}_f \tag{43}$$

$$L_f \frac{d\hat{i}_f}{dt} = \hat{v}_i - \hat{v}_f \tag{44}$$

$$C_f \frac{d\hat{v}_f}{dt} = \hat{i}_f - \hat{i}_L \tag{45}$$

$$\hat{i}_L = \frac{V_{con}}{K}\hat{v}_f \tag{46}$$

We can substitute V_{con} from (42) into (46) and simplify to get

$$\hat{i}_L = \frac{V_o^2}{RV_s^2}\hat{v}_f \tag{47}$$

Next, we can substitute (47) into (45), which yields

$$C_f \frac{d\hat{v}_f}{dt} = \hat{i}_f - \frac{V_o^2}{RV_s^2}\hat{v}_f \tag{48}$$

as our third dynamic equation.

8) AVERAGEING OVER HALF THE LINE PERIOD

Now, we take the average over half the line period for (43), (44), and (48). Taking this average only affects V_s, such that (43) and (44) are not affected and remain the same.

Using the large-signal relationship in (41) and the same mathematical development previously shown in (20) and (21), we see that V_s^2 averaged over half the line period is

$$\bar{V_s^2} = V_{rms}^2 \tag{49}$$

Then, substituting (49) into (48) yields the half-line-averaged small-signal equation which is

$$C_f \frac{d\hat{v}_f}{dt} = \hat{i}_f - \frac{V_o^2}{RV_{rms}^2}\hat{v}_f \tag{50}$$

9) LAPLACE TRANSFORM

Finally, the Laplace transform is applied to (43), (44), and (50), and like terms are gathered, which, respectively, yields

$$C_i s\hat{v}_i = \hat{i}_i - \hat{i}_f \tag{51}$$

$$L_f s\hat{i}_f = \hat{v}_i - \hat{v}_f \tag{52}$$

$$\left(C_f s + \frac{V_o^2}{RV_{rms}{}^2}\right)\hat{v}_f = \hat{i}_f \tag{53}$$

These equations represent the line-averaged (over half the line period) small-signal model for the PFC boost converter with an input filter, and will be used to derive the input impedance transfer function.

G. INPUT IMPEDANCE TRANSFER FUNCTION

Notice that (47) can be rearranged into the input impedance of only the boost converter (without the input filter), which is

$$\frac{\hat{v}_f}{\hat{i}_L} = \frac{RV_s{}^2}{V_o^2} \tag{54}$$

Then, applying averaging over half the line period and using the relationship given in (49) results in

$$\frac{\hat{v}_f}{\hat{i}_L} = R_{zi} = \frac{RV_{rms}{}^2}{V_o^2} \tag{55}$$

where we denote R_{zi} as the equivalent input resistance of the boost converter.

We use (55) to substitute R_{zi} into (53). Then, we solve the system of equations given in (51), (52), and (53) to find the transfer function in terms of $\hat{i}_i$ and $\hat{v}_i$. After careful calculation, the input impedance transfer function for the PFC boost converter with the simplifed input filter is expressed as

$$Z_i = R_{zi}\frac{L_f C_f s^2 + \frac{L_f}{R_{zi}}s + 1}{C_i L_f C_f R_{zi} s^3 + C_i L_f s^2 + (C_i + C_f)R_{zi}s + 1} \tag{56}$$

Although the input impedance is fully captured in (56), the small-signal diagram of the input impedance is shown in Fig. 11 for completeness.

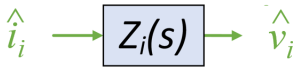

FIGURE 11. Small-signal diagram used to analyze the input impedance of the PFC boost converter from the ac-side, where the perturbation signal is the small-signal input current $\hat{i}_i$ and the response is measured at the voltage $\hat{v}_i$.

H. INPUT IMPEDANCE MODEL COMPARISON

The small-signal model for the input impedance, given in (56), can be used to generate the frequency response. Fig. 12 shows the input impedance frequency response, comparing the derived model with the simulation results using an ac source at rms voltages of 105 V, 185 V, and 265 V. Above twice the line frequency of 100 Hz, the ac-side model and simulation results are fairly well matched. The model slightly diverges from the simulation due to the simplification of the input filter in the model, but at frequencies above 5 kHz, the high-frequency filter characteristics are quite accurate. Around the line frequency (10-100 Hz), the injected small signals interact with the line frequency such that a magnitude peak occurs. This interaction is difficult to model and is not included in the derived ac-side model. Although the model is useful for evaluating the input impedance above the line-frequency interaction range, using an ac source in simulation is the recommended way to determine the accurate input impedance for a boost PFC converter over the full frequency range.

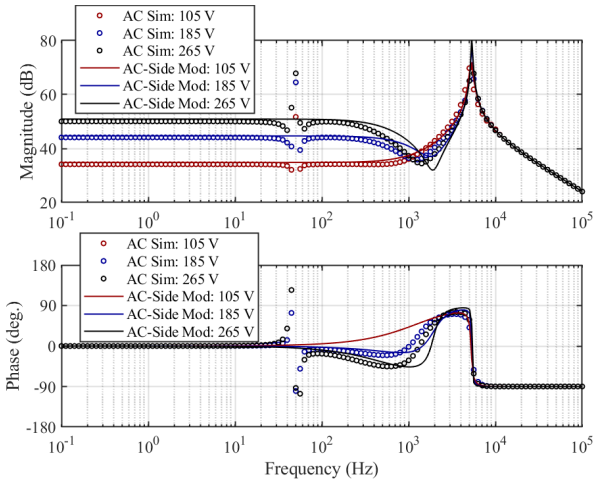

FIGURE 12. Frequency response of the input impedance simulated with an ac source for rms voltages of 105, 185, and 265 V compared to the ac-side PFC boost converter small-signal model with the same three rms values. The output voltage is 400 V at 0.5 A with a resistive load of 800 ohms for all input voltage cases.

V. DISCUSSION

Comparing the model and simulation results in Fig. 7 and Fig. 9 showed that the line-averaged rectified PFC boost converter model is accurate for the frequency responses of the control loop and output impedance. After averaging over half the line period, the input source voltage in transfer function (29) is mathematically equivalent to the source rms voltage, which means that the input ac source can be replaced with a dc source in simulation to produce equivalent Bode plot results. Although the early literature observed this relationship [20], [21], no other published papers explicitly derived this relationship, as done in this paper, to prove that the rms value is mathematically equivalent to the line-averaged source in the rectified PFC boost converter model. Looking back at the derivation, particularly from (7) to (11), this relationship with the rms value holds because the voltage v_f at the input of the boost converter stage is fed forward to the multiplier that produces the current reference value; without this, the relationship to the rms and the ability to replace the ac source with a dc source would not necessarily hold. However, since the presented control method is common for PFC implementation, these findings are profound for simplifying the analysis and simulation time to determine the control loop and output impedance of PFC boost converters.

For the input impedance of the PFC boost converter, the comparison of model and simulation results in Fig. 12 showed that the line-averaged ac-side PFC boost converter model is accurate for the input impedance frequency response, excluding the region around the line frequency. Unlike the line-averaged rectified model, the ac-side model focuses on the small signals before the rectifier so a dc source cannot directly replace the ac source for the input impedance frequency response, as shown in Fig. 4. Input impedance

has been modeled in previous literature, but the precise meaning of some early models can be difficult to navigate. For example, an early approach was to treat the ac source as a series of dc values ranging from 0 V to the maximum value of the ac line [23] (referred to as a piece-wise linear model in [24]), but this was found not to be equivalent to the input impedance in [24]. Similarly, a model in [25] examined the effect of amplitude modulation on the input impedance of the boost converter stage, which is not the same as the input impedance at the ac source. Other input impedance models have been developed that accurately capture the interaction with the line frequency [7], [26], but are more complex to model. Hence, despite the nontrivial simulation time, simulation with an ac source is an effective method to accurately determine the input impedance of the PFC boost converter over the full frequency range.

VI. CONCLUSION

Power factor correction converters for industrial applications often require extensive simulation to design and verify the PFC converter and its controller. In this study, a single-phase PFC boost converter with average current-mode feedback control (in CCM and with a high power factor) was simulated in SIMPLIS to investigate the ac analysis of its control loop, output impedance, and input impedance. The control loop (T) is used to verify the stability and dynamic performance of the converter through ac analysis. The output impedance (Z_o) and the input impedance (Z_i) are used to analyze the impedance interactions that determine system stability.

The small-signal models for the control loop and output impedance were derived using a line-averaged rectified model of the PFC boost converter, and the derived transfer functions matched the simulated results using either an ac or dc source. The small-signal model for the input impedance was derived using a line-averaged ac-side model of the PFC boost converter, and its frequency response matched the simulated results using an ac source.

The derivation and simulation results verified that a dc voltage source set to the rms value of the ac voltage source can be used for accurate ac analysis of the control loop (T) and the output impedance (Z_o). However, a dc source cannot be subsituted in the same way and an ac source should be used for accurate ac analysis of the input impedance (Z_i). The findings presented in this paper can aid in effective use of dc sources and ac sources during simulation to achieve accurate ac analysis results while minimizing simulation time.

APPENDIX A
SIMULATIONS PARAMETERS

For the small-signal modeling of the single-phase PFC boost converter operating in CCM shown in Fig. 1, all converter parameters, their variable names, and their values in this application are given in Table 3. Note that some values are neglected in the modeling.

TABLE 3. Complete converter parameters.

Parameter	Variable	Value
Output voltage	V_o	$400\,V$
Supply voltage (dc)	V_s	$105 - 265\,V$
Load resistance	R	$800\,\Omega$
Inductance	L	$2.2\,mH$
Capacitance	C	$180\,\mu H$
Switch on-resistance	r_{ds}	$3.9048\,\Omega$
Diode on-resistance	r_d	$0.01\,\Omega$
Diode voltage drop	V_d	$0.75\,V$
ESR of inductor	r_L	$0.1\,\Omega$
ESR of capacitor	r_c	$30\,m\Omega$
Filter inductor	L_3	$5\,mH$
Filter inductor resistance	R_{L3}	$100\,m\Omega$
Filter inductor	L_4	$5\,mH$
Filter inductor resistance	R_{L4}	$100\,m\Omega$
Filter capacitor	C_6	$220\,nF$
Filter capacitor	C_7	$100\,nF$
Filter capacitor	C_8	$470\,nF$
Filter capacitor	C_9	$4.7\,nF$
Filter capacitor	C_{10}	$4.7\,nF$
Filter resistor	R_4	$30\,m\Omega$
Filter resistor	R_5	$30\,m\Omega$
Filter resistor	R_9	$30\,m\Omega$
Filter resistor	R_{10}	$2\,M\Omega$
Filter resistor	R_{11}	$2\,M\Omega$
Feedforward divider	$1/K$	0.00411
Modulation factor	F_m	0.2
Voltage sensor factor	R_v	0.0075
Voltage compensator capacitor	C_2	$490\,nF$
Voltage compensator capacitor	C_3	$120\,nF$
Voltage compensator resistor	R_2	$20\,k\Omega$
Voltage compensator resistor	R_3	$20\,k\Omega$
Current sensor factor	R_i	1
Current compensator capacitor	C_4	$22\,nF$
Current compensator capacitor	C_5	$820\,pF$
Current compensator resistor	R_6	$1.8\,k\Omega$
Current compensator resistor	R_7	$3.3\,k\Omega$

APPENDIX B
ONLINE RESOURCES

Downloadable files of the SIMPLIS schematic and Matlab files are available at: http://pearslab.net/pfc-boost/ .

CONFLICT OF INTEREST STATEMENT

Katherine A. Kim received a research grant from SIMPLIS Technologies, Inc., in 2020–2021 to partially support this research. Thomas G. Wilson Jr. is the President of SIMPLIS Technologies, Inc.

ACKNOWLEDGMENT

The authors would like to sincerely thank Guan-Ru Li and Ting-Yu Lin, who contributed to the preliminary research for this work, and Christophe Basso and Mauricio Cespedes for their feedback on the early versions of this article

REFERENCES

[1] O. Garcia, J. A. Cobos, R. Prieto, P. Alou, and J. Uceda, "Single phase power factor correction: A survey," *IEEE Trans. Power Electron.*, vol. 18, no. 3, pp. 749–755, May 2003.

[2] *Electromagnetic Compatibility (EMC)—Part 3-2: Limits—Limits for Harmonic Current Emissions*, Standard IEC 61000-3-2, 2018.

[3] A. Fernandez, J. Sebastian, M. M. Hernando, P. Villegas, and J. Garcia, "Helpful hints to select a power-factor-correction solution for low- and medium-power single-phase power supplies," *IEEE Trans. Ind. Electron.*, vol. 52, no. 1, pp. 46–55, Feb. 2005.
[4] J.-Y. Lee, J.-H. Chen, and K.-Y. Lo, "Design of a GaN totem-pole PFC converter using DC-link voltage control strategy for data center applications," *IEEE Access*, vol. 10, pp. 50278–50287, 2022.
[5] S. S. Sayed and A. M. Massoud, "Review on state-of-the-art unidirectional non-isolated power factor correction converters for short-/long-distance electric vehicles," *IEEE Access*, vol. 10, pp. 11308–11340, 2022.
[6] K.-W. Heo, J. Jin, and J.-H. Jung, "Maximum voltage gain tracking algorithm for high-efficiency of two-stage induction heating systems using resonant impedance estimation," *IEEE Trans. Ind. Electron.*, vol. 70, no. 8, pp. 7934–7943, Aug. 2023.
[7] J. Sun, M. Xu, M. Cespedes, and M. Kauffman, "Data center power system stability—Part I: Power supply impedance modeling," *CSEE J. Power Energy Syst.*, vol. 8, no. 2, pp. 403–419, Mar. 2022.
[8] J. Sun, M. Mihret, M. Cespedes, D. Wong, and M. Kauffman, "Data center power system stability—Part II: System modeling and analysis," *CSEE J. Power Energy Syst.*, vol. 8, no. 2, pp. 420–438, Mar. 2022.
[9] T. Busatto, S. K. Rönnberg, and M. H. J. Bollen, "Stability analysis of PFC converters under different source impedances and its consequences on zero-crossing distortion," *IEEE Trans. Power Del.*, vol. 37, no. 4, pp. 3235–3244, Aug. 2022.
[10] T. Zhu, X. Wang, F. Zhao, and G. V. Torrico-Bascopé, "Impedance analysis and resonance mitigation for boost PFC converters using sample correction," *IEEE Trans. Power Electron.*, vol. 38, no. 12, pp. 15214–15224, Dec. 2023.
[11] B. Choi, S.-S. Hong, and H. Park, "Modeling and small-signal analysis of controlled on-time boost power-factor-correction circuit," *IEEE Trans. Ind. Electron.*, vol. 48, no. 1, pp. 136–142, Jun. 2001.
[12] B. Bryant and M. K. Kazimierczuk, "Open-loop power-stage transfer functions relevant to current-mode control of boost PWM converter operating in CCM," *IEEE Trans. Circuits Syst. I, Reg. Papers*, vol. 52, no. 10, pp. 2158–2164, Oct. 2005.
[13] B. Choi, *Pulsewidth Modulated DC-to-DC Power Conversion Circuits, Dynamics, and Control Designs*. Hoboken, NJ, USA: Wiley, 2013.
[14] R. D. Middlebrook, "Input filter considerations in design and application of switching regulators," in *Proc. Rec. IEEE Ind. Appl. Soc. Annu. Meeting*, Jun. 1976, pp. 366–382.
[15] C. D. Davidson and R. Szasz, "Compatibility of switchmode rectifiers with engine generators," in *Proc. 22nd Int. Telecommun. Energy Conf. (INTELEC)*, Sep. 2000, pp. 626–631.
[16] S.-Y. Chiu and K. A. Kim, "System analysis and design for multiconverter electrical power systems in nanosatellites," *IEEE J. Miniaturization Air Space Syst.*, vol. 4, no. 1, pp. 41–53, Mar. 2023.
[17] J. Sun, "Impedance-based stability criterion for grid-connected inverters," *IEEE Trans. Power Electron.*, vol. 26, no. 11, pp. 3075–3078, Nov. 2011.
[18] J. Moldaschl, J. Broulím, and L. Palocko, "Boost power factor correction topology with average current control," in *Proc. Int. Conf. Appl. Electron.*, Sep. 2014, pp. 213–216.
[19] R. W. Erickson and D. Maksimovic, *Fundamentals of Power Electronics*, 2nd ed., Norwell, MA, USA: Kluwer, 2001.
[20] F. A. Huliehel, F. C. Lee, and B. H. Cho, "Small-signal modeling of the single-phase boost high power factor converter with constant frequency control," in *Proc. PESC Rec. 23rd Annu. IEEE Power Electron. Spec. Conf.*, Jun. 1992, pp. 475–482.
[21] K. Chan Lee and B. H. Cho, "Design of the feedback loop for single controller power factor correction converter," in *Proc. PESC Rec. 29th Annu. IEEE Power Electron. Spec. Conf.*, vol. 1, May 1998, pp. 899–904.
[22] W. Zhong, S. Bai, and C. Hu, "Power factor correction modulated wireless power transfer system with series-series compensation," *IEEE Access*, vol. 11, pp. 17576–17583, 2023.
[23] R. Redl and A. S. Kislovski, "Source impedance and current-control loop interaction in high-frequency power-factor correctors," in *Proc. PESC Rec. 23rd Annu. IEEE Power Electron. Spec. Conf.*, Jun. 1992, pp. 483–488.
[24] J. Sun, "Input impedance analysis of single-phase PFC converters," *IEEE Trans. Power Electron.*, vol. 20, no. 2, pp. 308–314, Mar. 2005.
[25] M. Chen and J. Sun, "Low-frequency input impedance modeling of boost single-phase PFC converters," *IEEE Trans. Power Electron.*, vol. 22, no. 4, pp. 1402–1409, Jul. 2007.
[26] V. Salis, A. Costabeber, P. Zanchetta, and S. Cox, "A generalised harmonic linearisation method for power converters input/output impedance calculation," in *Proc. 18th Eur. Conf. Power Electron. Appl. (EPE ECCE Eur.)*, Sep. 2016, pp. 1–7.

KATHERINE A. KIM (Senior Member, IEEE) received the B.S. degree in electrical and computer engineering from the Franklin W. Olin College of Engineering, Needham, MA, USA, in 2007, and the M.S. and Ph.D. degrees in electrical and computer engineering from the University of Illinois at Urbana–Champaign, Champaign, IL, USA, in 2011 and 2014, respectively.

In 2014, she started as an Assistant Professor of electrical and computer engineering with Ulsan National Institute of Science and Technology (UNIST), Ulsan, South Korea. Since 2019, she has been with National Taiwan University, Taipei, Taiwan, where she is currently a Professor of electrical engineering. Her research interests include power electronics and control for solar photovoltaic applications.

Dr. Kim received the Award for Achievements in Power Electronics Education from the IEEE Power Electronics Society (PELS), in 2022, recognition as an Innovator Under 35 for Asia Pacific Region by the MIT Technology Review, in 2020, and the Richard M. Bass Outstanding Young Power Electronics Engineer Award from PELS, in 2019. Since 2017, she has served as an Associate Editor for IEEE TRANSACTIONS ON POWER ELECTRONICS. For IEEE PELS, she served as the Student Membership Chair, from 2013 to 2014, a PELS Member-at-Large, from 2016 to 2018, the PELS Women in Engineering Chair, from 2018 to 2020, and the PELS Constitution and Bylaws Chair, from 2021 to 2023. She is currently the IEEE PELS Vice President of Global Relations, from 2024 to 2025.

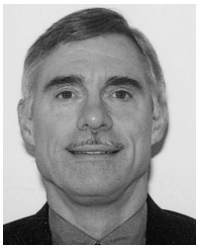

THOMAS G. WILSON JR. (Member, IEEE) received the A.B. degree from Harvard University, in 1972, and the M.Eng. and D.Eng. degrees from the University of California at Berkeley, Berkeley, CA, USA, in 1974 and 1977, respectively.

He is currently the President of SIMPLIS Technologies, Inc. and the Technology Leader of Simulation Software at the Power Electronics Industry. He worked for 20 years at AT&T Bell Labs as a Power Supply Designer, the Design Manager, the Manufacturing Manager, the Marketing Manager, and the Applications Manager. In 1994, he left AT&T to become a Chief Engineer at Zytec Corporation. In 2000, he joined Transim Technology Corporation as the Vice President of Engineering. SIMPLIS Technologies was spun off from Transim, in 2008. He has authored and co-authored 20 IEEE publications in the field of power electronics and holds seven U.S. patents. He has served two terms as the Technical Vice President of the PELS Administrative Committee. He was the Conference Chair of the Applied Power Electronics Conference (APEC), in 1997, and a member and then the Chair of the APEC Steering Committee.